JOURNAL OF MATERIALS SCIENCE: MATERIALS IN MEDICINE **10** (1999) 309–317

Fracture evaluation of acrylic bone cements modified with hydroxyapatite: influence of the storage conditions

P. MONTEMARTINI, T. CUADRADO, P. FRONTINI*
Institute of Materials Science and Technology-INTEMA, (CONICET-UNMdP) J.B. Justo 4302-7600, Mar del Plata, Argentina

Fracture and mechanical characterization of bone composite composed of polymethylmethacrylate and hydroxyapatite (HA) at different contents was carried out. Hydroxyapatite is added in order to improve cement biocompatibility, but it is expected that it also affects mechanical properties. Specimens were either stored in air at 37 °C for 120 h or in physiological solution (PhS-37), in order to establish the influence of storage conditions upon mechanical behavior. One set of specimens was also postcured at 120 °C for 4 h to take into account the influence of free monomer. Fracture experiments revealed some non-linearity in load–displacement records and differences in trends between initiation and propagation values of the fracture surface energies. The trends in the data shows that HA acts as a rigid filler enhancing fracture resistance, flexural modules and yield stress, up to a certain content. Beyond the latter limit, properties suffer a deterioration because the addition of HA also affects the cement porosity. Absorbed water acts as plasticizer leading to a decrease in mechanical properties. The highest propagation strain energies were exhibited by materials aged in PhS-37.

1. Introduction

Polymethyl methacrylate (PMMA) bone cements, introduced in 1960, improved the performance of joint implants giving a more even distribution of interface stresses. However the problem of deterioration of the polymer–bone or polymer–metal interface with time leading to implant mechanical instability remains unsolved.

Failure can be due to a number of factors. Wear is one of the main problems associated with materials used in implants: wear metallic or polymeric (PMMA, high density polyethylene (HDPE)) particles become incorporated into the surrounding tissues, causing bone resorption and eventual loosening after time. By using a radio-opaque cement Weber and Charnley [1] were able to observe for the first time fractures of acrylic cement around the femoral stem of total hip prosthesis.

Many investigators thus attempted to modify PMMA in order to improve long-term fracture strength and to increase the mechanical interlocking with bone by introducing fibers [2, 3], controlled porosity [4, 5] and recently surface-reactive fillers such as hydroxyapatite (HA) [6]. HA is the main mineral component of calcified tissues and it is known to be totally biocompatible [7, 8] and to form a direct bond with the neighboring bone.

The capability of different modifications upon final properties of the cement are usually evaluated by critical stress intensity factor, K_{IC}.

However, results appear to be contradictory. For instance, Beaumont and Young [9] reported the adverse effect of porosity on K_{IC} of Simplex P bone cement, showing 46% increase (1.68 versus 1.15 MPa) in fracture resistance of cements cured under pressure of 0.71 rather than 0.07 MPa. In contrast to these findings, Rimnac *et al.* [4] reported no significant enhancement in the fracture toughness for cements formed using centrifugation while Wang and Pilliar [5] showed that an increase in porosity (1.6–5.2%) resulted in an increase in K_{IC} (1.01–1.26 MPa).

We believe that differences in K_{IC} values can arise from the lack of standardized procedure neither for the specimen preparation nor for the conditioning for acrylic bone cements; for instance, different authors calculate K_{IC} from samples in conditions varying between 4 to 25 mm width and conditioned in air or in physiological solution from 20 to 37 °C [2–4, 10–12].

It is well known that crazing and fracture properties of polymers are strongly influenced by the environment: crazing due to chemical effects, crack tip plasticizing by liquids, molecular mobility modification by hydrostatic liquid pressure. It was reported that when unnotched samples cut from PMMA, which was previously saturated with water, are broken in air it appears that the brittleness increases at higher water content because of the appearance of water cluster in the material [13]. Hailey *et al.* [14] also reported the influence of long-term

*Author to whom correspondence should be addressed.

storage conditions on fracture resistance upon unmodified cements. On the other hand, the samples' dimensions determine the free monomer content, as it is related to the rise in temperature during polymerization [15]. The latter statements indicate that storage conditions and sample dimensions are expected to be very important in determining properties. This paper aims to gain more insight upon the influence of aging conditions upon mechanical and fracture behavior of HA modified acrylic bone cements.

2. Materials and methods

2.1. Sample preparation

Subiton^{TM} (Subiton Laboratories S.R.L.) radio-opaque bone cement and synthetic HA powder was used in the present study. The cement consisted of PMMA powder with 2.4% initiator (benzoyl peroxide; BPO) and 10% barium sulfate; the monomer MMA containing 1.2% (in weight) *N,N*-dimethyl-*p*-toluidine and traces of hydroquinone. The filler, HA, was synthesized through the modified precipitation method from orthophosphoric acid (H_3PO_4) solution and a calcium hydroxide ($Ca(OH)_2$) suspension containing NH_4OH [15].

HA powder particle size distributions (D_p equal to 13 μm), Ca/P ratio (1.67) and the nature of the crystalline phases present was determined as described elsewhere [17].

In order to investigate the influence of HA different weight fractions of powder were achieved by removing PMMA polymer from the 40 g of powder and replacing with equal weight of HA particles.

Monomer and modified powder were hand-mixed, according to the manufacturer's instructions (2:1 modified powder/liquid), at approximately 0.5 Hz in a bowl for 2–3 min.

Before the doughing time had been reached the mix was poured into a glass mold to obtain a sheet of cement (4.5 × 100 × 200 mm). After curing for 40 min under minimal pressure, these sheets were removed from the mold. Test beams (4.5 × 80 × 10 mm) were cut from them. The specimens of each HA percentage were divided into three subgroups and they were aged following different policies for 120 h. One subgroup of specimens was completely cured by annealing at 120 °C for 4 h and then they were placed at 37 °C for 116 h in air (A-120). The second subgroup was aged in the incubator at 37 °C for 120 h in air (A-37) and the last one was soaked in physiological solution (PhS) at 37 °C for 120 h (PhS-37).

The residual monomer content was determined using a Hewlett Packard Serie II gas chromatograph with flame ionization detection. The detector temperature was 200 °C and the oven temperature was 180 °C. Nitrogen carrier gas was used at a flow rate of 18.4 $cm^3\,min^{-1}$ through a stainless steel column (3.05 m length; 3 mm diameter) containing a stationary phase of Emulphor ON 870 supported on Chromosorb W. Dichloromethane was used as the solvent of the polymer. A sample of approximately 1 g of cement was weighed out and the weight recorded accurately. The cement sample was then dissolved in 25 ml of dichloromethane at room temperature. Then, the solution was left for 12 h to ensure dissolution and to allow the barium sulfate to settle out. Samples free monomer content are indicated in Table I.

2.2. Mechanical properties

Flexural modulus was determined in three-point bending using sample dimensions recommended by ASTM D 790 standards (4.5 × 80 × 10 mm with a span to depth ratio of 15) at constant crosshead speed of 2 $mm\,min^{-1}$.

Compression engineering stress yielding was calculated in accordance with ISO 5833-92 from rectangular specimens (5 × 5 × 10 mm).

2.3. Fracture characterization

After storage and immediately prior to testing the bars for fracture resistance determination were notched using a razor blade having an on-edge tip radius of 13 μm, which ensures a sharp crack tip and, hence, very high stress concentrations at the tip. A minimum of five specimens of each program were tested in a Shimadzu Autograph test machine using the three-point bending method, single eddged notch beam (SENB) geometry (Fig. 1), in air at 20 °C and a constant crosshead speed of 10 $mm\,min^{-1}$.

The lack of published standards for the measurement of fracture toughness of acrylic cements makes it difficult to select *a priori* the width of the test specimen. The strength of materials is usually measured in plane strain because for this condition the fracture parameters are independent of the specimen size. Using a yield strength of 70 MPa and fracture toughness of 1.5 $MPa\,m^{1/2}$, a minimum specimen width of 1.2 mm was calculated via the size criteria

$$B, a, (W - a) \geq 2.5\left(\frac{K_{IC}}{\sigma_Y}\right)^2 \quad (1)$$

Then, 4.5 mm width specimens were used, which greatly exceed the minimum size required.

Values of K_{IC} were computed using the method described in Williams and Cawood [18] for SENB geometry, from

$$K_{IC} = \frac{fP_Q}{BW^{1/2}} \quad (2)$$

where

$$f = 6\left(\frac{a}{W}\right)^{(1/2)} \frac{\left\{1.99 - \left(\frac{a}{W}\right)\left(1 - \frac{a}{W}\right)\left[2.15 - 3.93\left(\frac{a}{W}\right) + 2.7\left(\frac{a}{W}\right)^2\right]\right\}}{\left[1 + 2\left(\frac{a}{W}\right)\right]\left[1 - \left(\frac{a}{w}\right)\right]^{3/2}} \quad (3)$$

where P_Q = load at crack initiation; B, a, W = specimen dimensions (Fig. 1).

TABLE I Monomer content of stored samples

Storage conditions	Free monomer (%) (w/w)
A-37	3.1
A-120	1.1
PhS-37	2.4

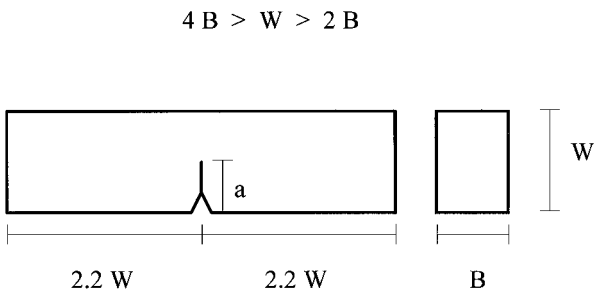

Figure 1 Fracture test configuration.

When the curve of load versus load point displacement is a straight line with an abrupt drop of load to zero at the instant of crack initiation, P_Q is the maximum load (Fig. 2a). However, when some non-linearity is displayed the true initiation load is not defined by the maximum and an arbitrary rule is generally used [13]. The diagram is shown (exaggerated) in Fig. 2b and the best straight line should be drawn to determine the initial compliance C as shown. This value is then increased by 5% and a further line drawn. If P_{max} falls within these two lines, then P_{max} is used to find K_{IC}. If $C_{+5\%}$ intersects the load curve, then $P_{5\%}$ is found and this is taken as the load at crack initiation.

The strain energy release rate was evaluated at its initiation value G_{CI} and its propagation value G_{CP}, following the methodology proposed by Adams *et al.* [19]. They were calculated from

$$G_{CI} = U_i/BW\phi \tag{4}$$

and

$$G_{CP} = U_P/B(W - a) \tag{5}$$

where U_i is the energy to initiate fracture, taken at the point of maximum force, ϕ is a calibration factor which is a function of a/W and L/W; and U_P is the total fracture energy.

2.4. Microscopy

Fracture surfaces were examined by scanning electron microscopy (SEM; Jeol JSM 35 CF apparatus), after coating the broken surfaces with a thin gold layer.

The porosity of HA modified cements were examined by image analysis (Image NHI 1.58) from optical microscopy of specimens included in epoxy resin.

3. Results and discussion

Table I shows the free monomer contents of all the samples tested. It can be seen that A-120 aging history effectively diminished the free monomer content. This annealing simulates the situation in thicker specimens, such as 25 mm thick specimens, where the center sample temperature reaches values of about 100 °C because of quasi-adiabatic conditions, as shown in Fig. 3 leading to higher degrees of polymerization.

The mass increment of samples submitted to PhS-37 aging history was measured with an analytical balance and the weight gain was calculated according to the equation

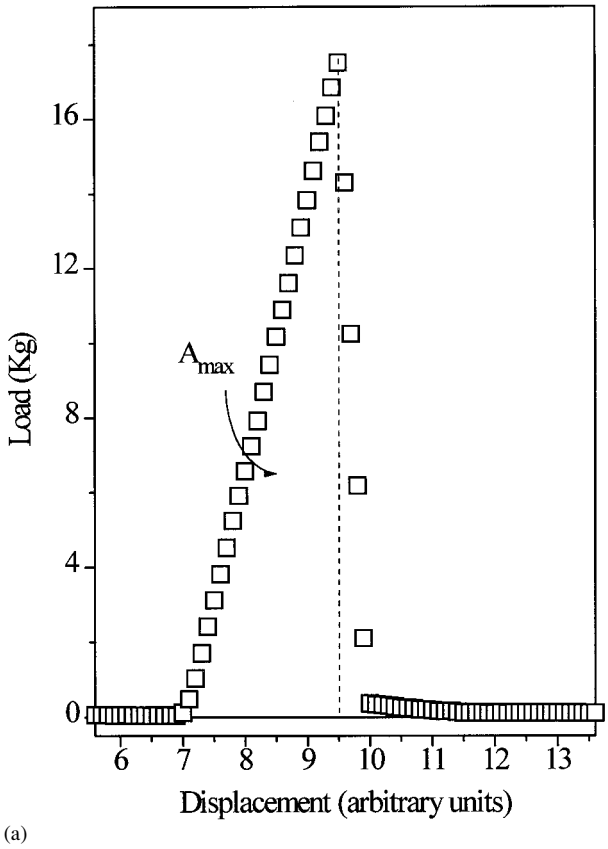

(a)

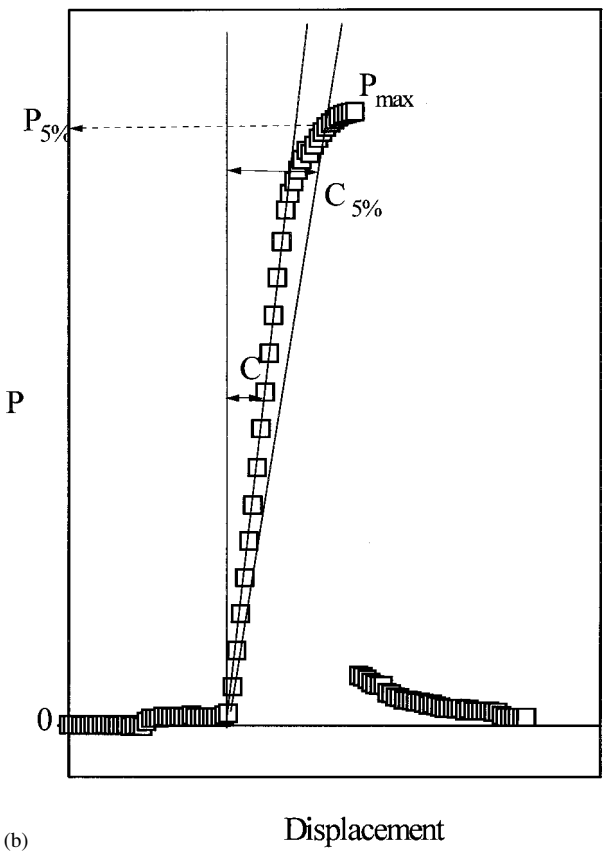

(b)

Figure 2 (a) Typical straight line load–displacement experiment. (b) A load–displacement experiment showing deviations from linearity.

$$\text{net mass increment} = \frac{\text{weight of specimen} - \text{weight of dry specimen}}{\text{weight of dry specimen}} \times 100 \tag{6}$$

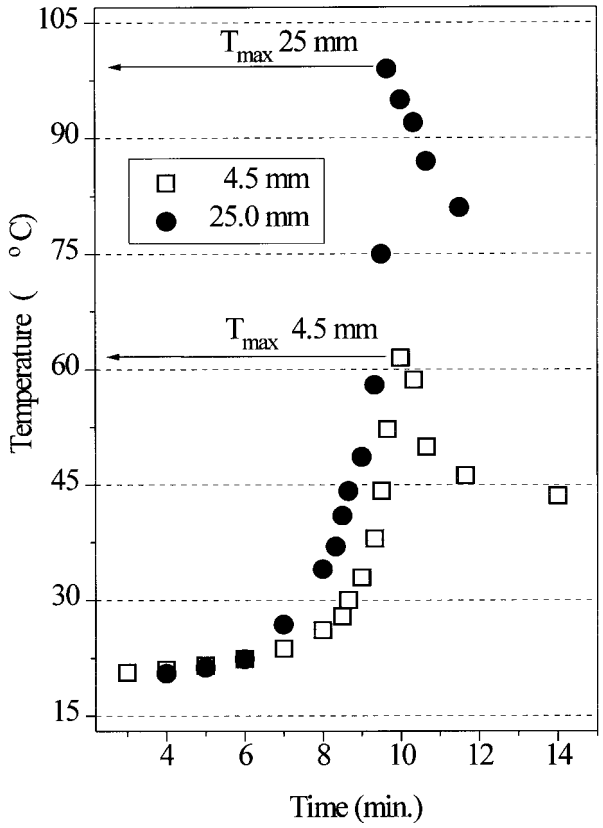

Figure 3 Temperature evolution during quasi-adiabatic curing.

The net mass increment was approximately 0.8% arising from the mass balance between water absorption and monomer leaching, irrespective of the HA content.

The addition of HA also affects material porosity. At HA levels higher than 5% the increase in porosity is important (Table II). This is a consequence of the large increase in dough viscosity during hand-mixing promoted by the incorporation of HA, which stops the air bubbles embodied during mixing from escaping. A large number of disjointed particles are also present in samples having high HA content. Fig. 4 shows HA particles settled on PMMA beads, diminishing the effective interfacial area available for chemical bonding between PMMA beads and the acrylic matrix.

Figs 5 and 6 show the flexural modulus (E) and compression yield stress (σ_Y) as a function of the HA amount for different storage conditions. Both properties exhibit a maximum of 2–5% in the case of A-37 specimens (Table III). The maximum observed in mechanical properties with HA content is consistent with results reported previously by Castaldini *et al.* [6] The increase in properties with HA content seems to be associated with the reinforcement action of HA which

TABLE II Percentage porosity

HA (%)	Porosity (%)
0	3.5
2	7.6
5	13.1
10	18.2

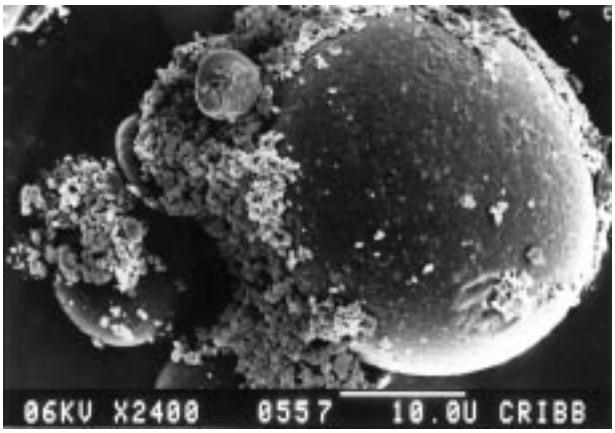

Figure 4 Micrograph showing the deposits of HA on PMMA beads surface.

acts as a rigid filler while the decrease beyond 5% may be associated with the large porosity levels induced by the modification with HA, as explained above.

A-120 aging program (postcuring) also enhances E and σ_Y consistent with the elimination of free monomer (Table I) which acts as a plasticizer [20]. In postcured materials HA reinforcement action appears to be negligible as materials displayed practically the same values of E and σ_Y irrespective of the HA content. (Figs 5 and 6, and Table III)

It has been stated that the modulus of elasticity and yield stress are highly dependent on the plasticizer content [8]; decreasing when plasticizers, residual monomer and/or water, increase. Consistent with these latter statements samples submitted to PhS-37 aging treatment display the lowest values of E and σ_Y at HA percentage range studied. (Figs 5 and 6, and Table III).

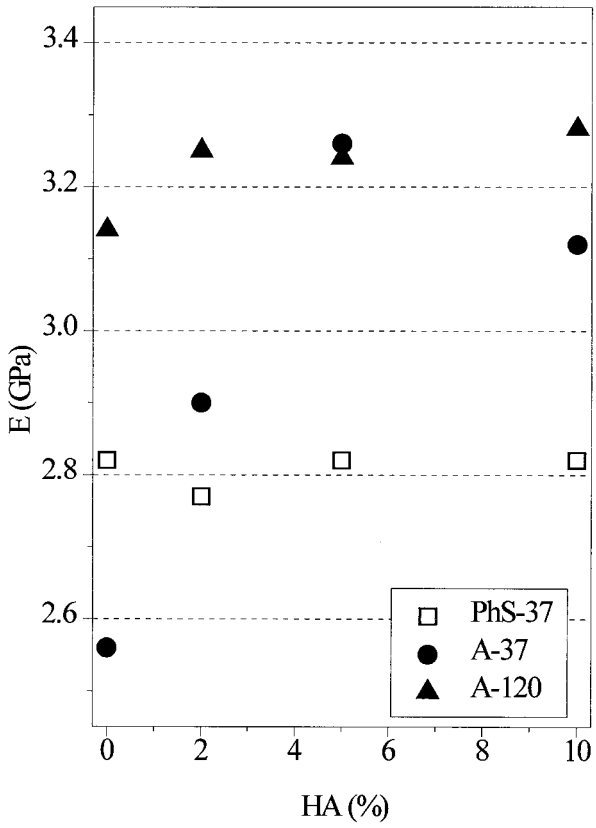

Figure 5 Flexural modulus against HA content.

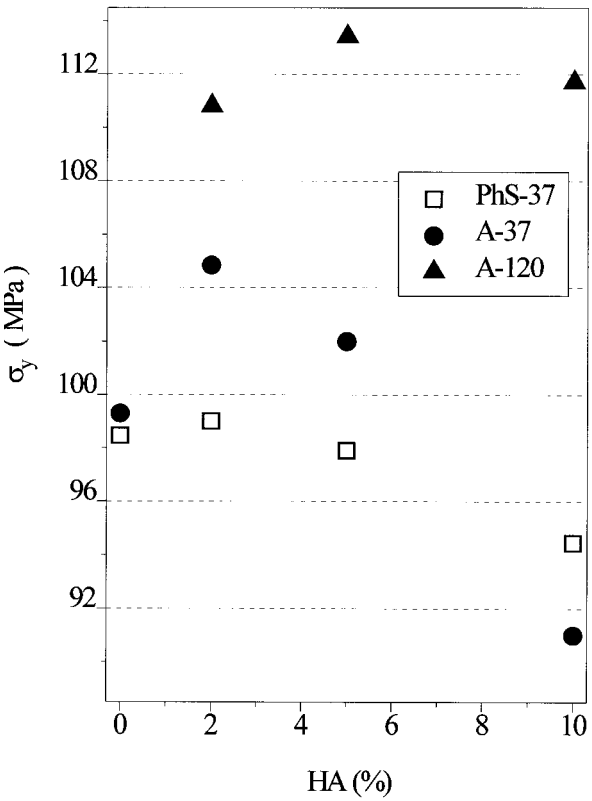

Figure 6 Compression yield strength against HA content.

The fracture surfaces are, macroscopically, very rough indicating rapid crack propagation and considerable crack branching. In the case of samples without HA (see Figs 7a, 8a and 9a) it is possible to observe PMMA beads well bonded to the matrix. This effect is stronger in A-120 samples (see Fig. 9a). Postcuring interbead matrix covers practically the entire bead surface due to the high degree of polymerization reached by the matrix during postcuring. Failure could be considered cohesive. In contrast, a different surface pattern was displayed by HA-modified samples (see Fig 7b, c, 8b, c, 9b, c). Very few PMMA particles are visible. Visual inspection of the micrographs reveals stress whitening due to interbead matrix drawing and particle debonding induced by the lower intrinsic strength of the particle–matrix interface.

In commercial PMMA (Plexiglas^{TM}) the curve of load versus load point displacement is a straight line with an abrupt drop of load to zero at the instant of crack initiation (Fig. 2a). In contrast, some non-linearity was displayed by our acrylic bone cements even though plane strain conditions were always met. This can be interpreted in terms of stable crack growth after initiation but prior to instability. This particular behavior is a consequence of the composite nature of the materials studied here.

In fact, the analysis of load–displacement records show that depending on the aging history samples exhibited a range of fracture stability ranging from a modest non linearity in load–displacement records to an unstable fracture with crack arrest regime. In Fig. 10 we present typical load–displacement curves obtained in single-notched three-point bending tests of an A-37 specimen without HA, a 10% HA A-120 specimen and a 10% PhS-37 specimen showing up crack propagation regimes.

Fig. 11 shows K_{IC} as a function of HA amount for different storage conditions.

Initiation values seems to be the result of the simultaneous action of HA reinforcing, plasticizers and porosity. HA seems to act as a reinforcement filler like $BaSO_4$ which is commonly added as a radio-opaque agent. It was argued that by the action of the rigid particulate filler such as $BaSO_4$ (or as in our case, HA) the toughness of the acrylic matrix is enhanced by promoting interactions between the moving crack front and the second phase dispersion, like the secondary fracture coalescence mechanism proposed by Lednicky and Pezbauer or by other mechanisms called ''crack pining'' [20].

It is known that the presence of monomer acts as a plasticizer in radiolucent cements due to plastic deformation induced at lower levels of stress in the crack tip (crack tip blunting) [20]. Even though, differences between A-37 and A-120 samples were found: it seems that the $BaSO_4$ reinforcement effect hindered the action of plasticizers. K_{IC} at 0% of HA are the same for A-37 and A-120 samples (Fig. 11 and Table IV). Initiation fracture resistance values of PhS-37 samples [4, 8] were lower. Results shown in Fig. 11 reveal that water uptake does not produce improvement of K_{IC} and an approximately constant value is observed for all samples with different HA weight fraction immersed in PhS, in contrast with the maximum observed for A-37 and A-120 specimen (Table IV).

Differences in fracture propagation mode are not reflected in K_{IC}. In order to take into acount for the differences in crack propagation mode found, propagation energy strain energy release rate was also calculated as proposed by Adams *et al*. [19] and Hailey *et al*. [14] who also found similar behavior in other materials.

A deeper analysis of load versus displacement graph, shown in Fig. 10, reveals that the propagation part of the total energy are larger for PhS-37 samples.

Differences between trends displayed by initiation and

TABLE III Flexural modulus (GPa) and compression stress yielding (MPa) of stored samples

HA	A-37		A-120		PhS-37	
(%)	σ_Y (MPa)	E (GPa)	σ_Y (MPa)	E (GPa)	σ_Y (MPa)	E (GPa)
0	99.3 ± 0.4	2.56 ± 0.03	–	3.14 ± 0.03	98.4 ± 1.3	2.82 ± 0.05
2	104.8 ± 5.0	2.90 ± 0.05	110.8 ± 3.9	3.25 ± 0.09	99.0 ± 1.7	2.77 ± 0.05
5	102.0 ± 2.1	3.26 ± 0.07	113.4 ± 1.5	3.24 ± 0.11	97.9 ± 0.9	2.82 ± 0.09
10	91.0 ± 2.5	3.12 ± 0.04	111.7 ± 1.0	3.28 ± 0.07	94.5 ± 0.5	2.82 ± 0.09

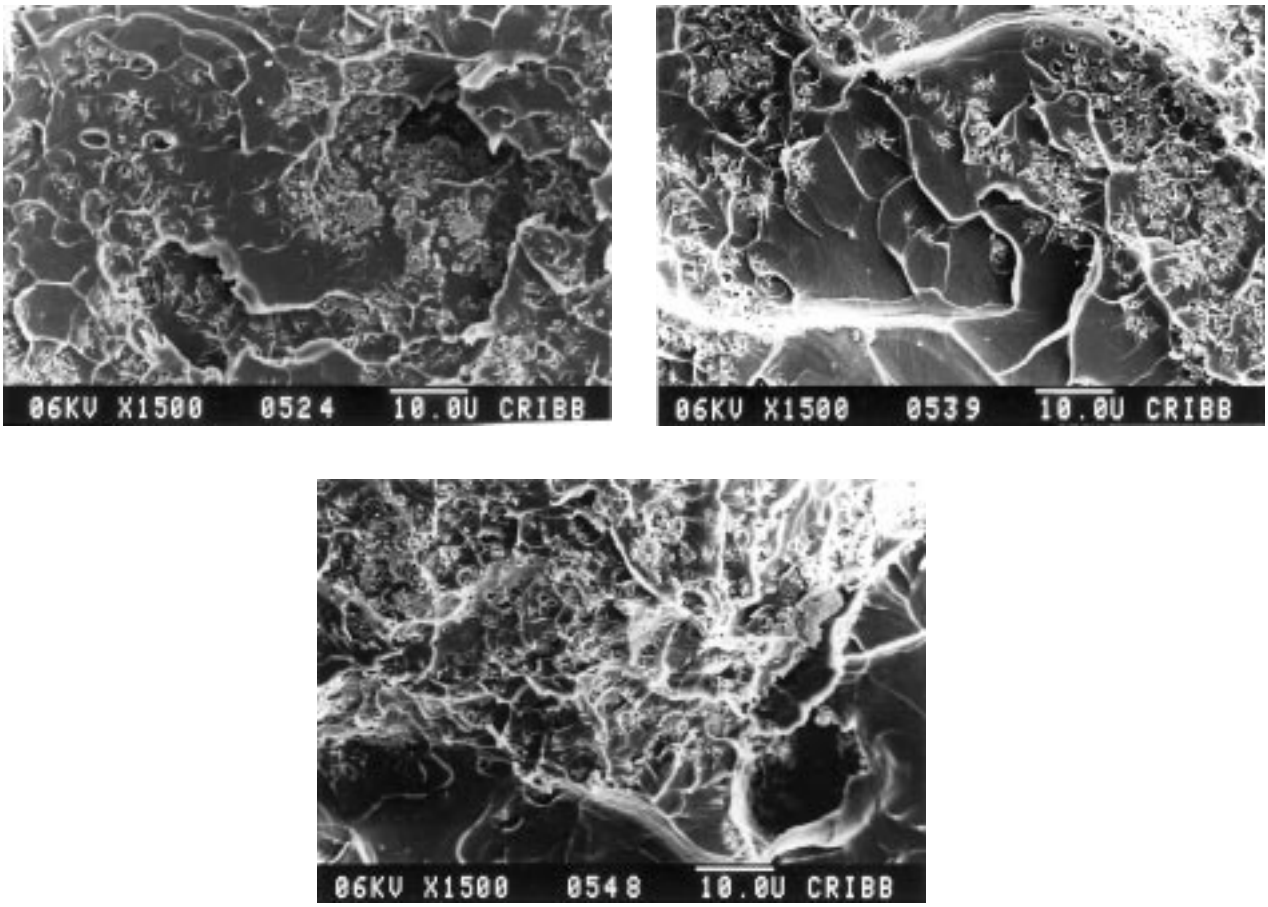

Figure 7 Fracture surfaces of PhS-37 samples with different HA content: (a) without HA, (b) 5% and (c) 10%.

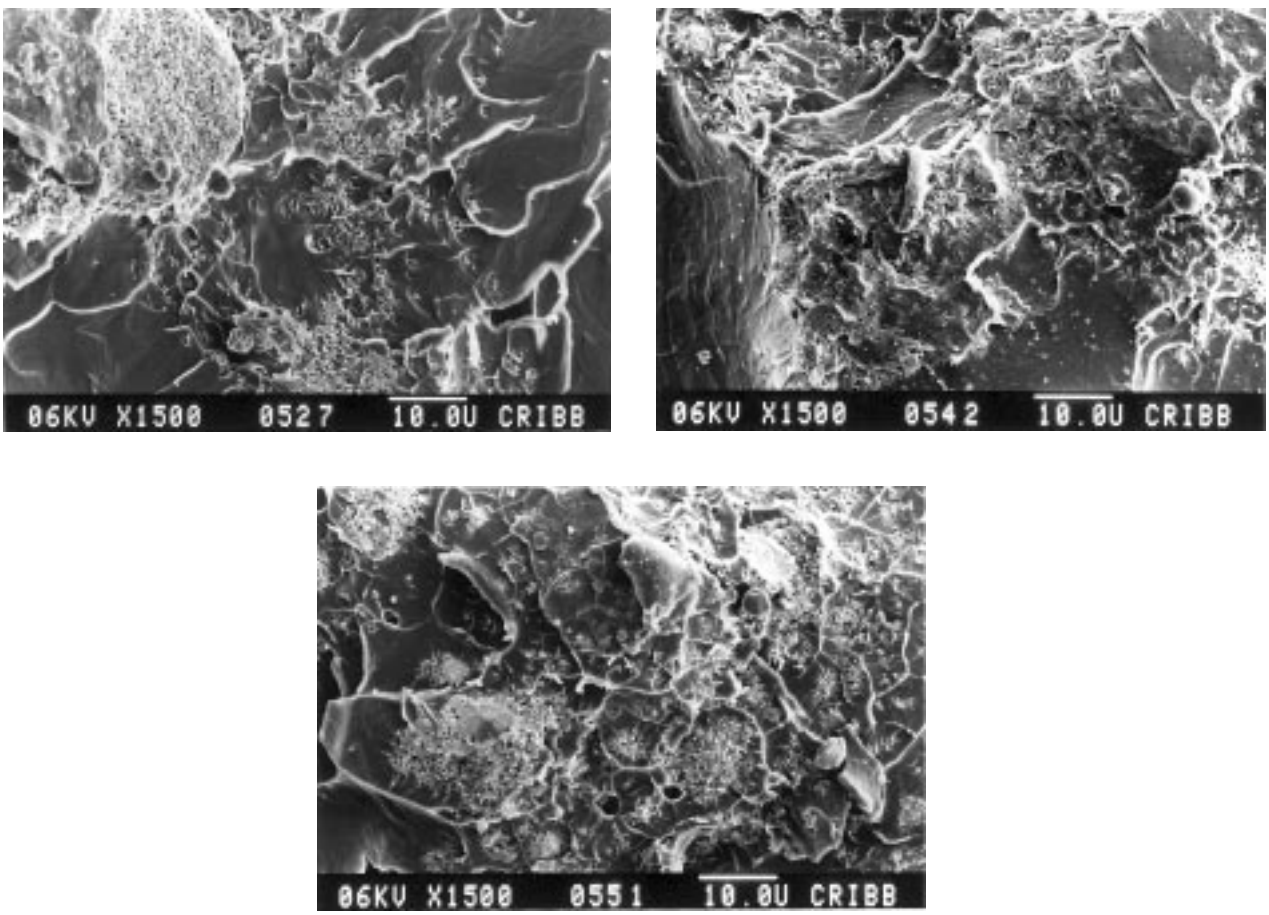

Figure 8 Fracture surfaces of A-37 samples with different HA content. (a) without HA, (b) 5% and (c) 10%.

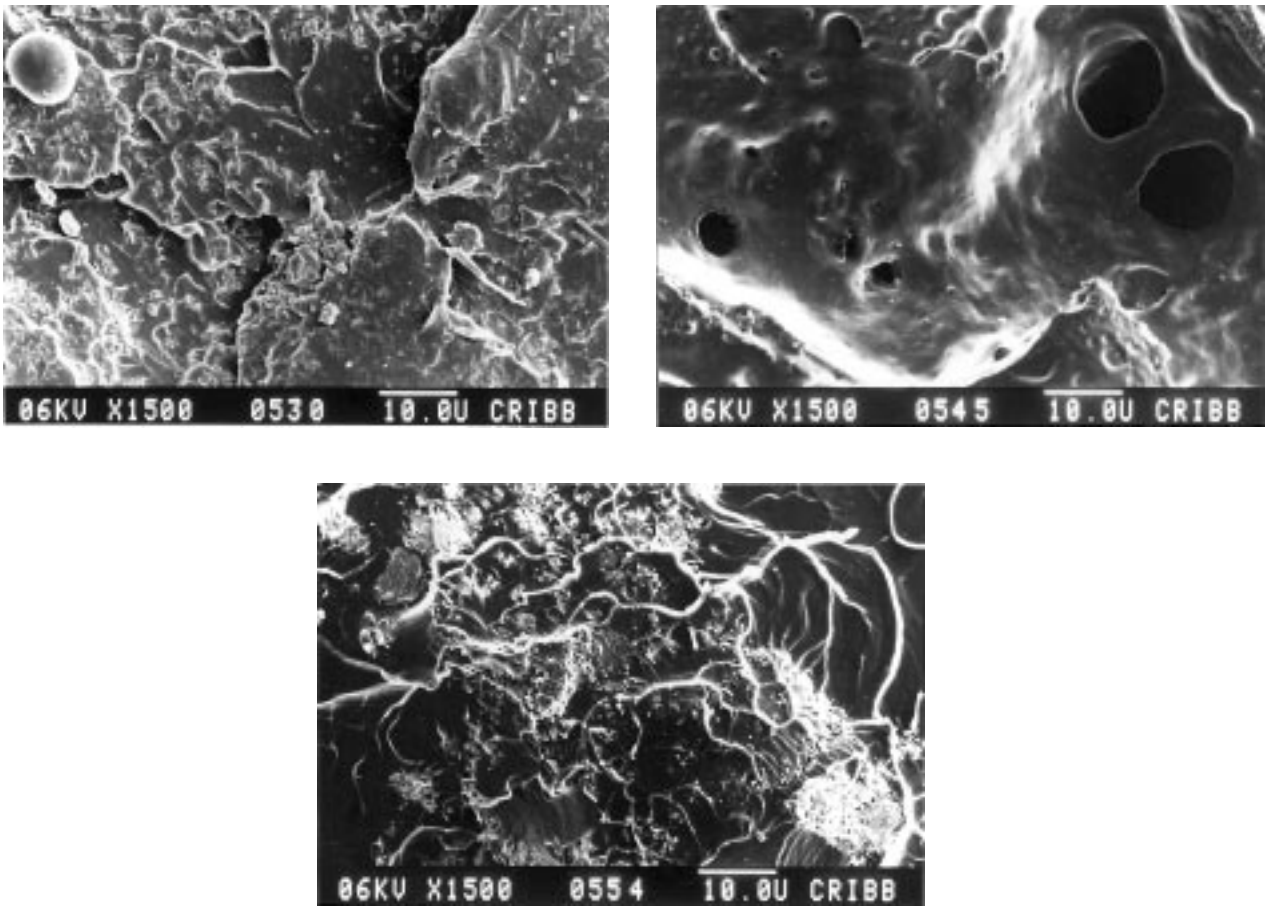

Figure 9 Fracture surfaces of A-120 samples with different HA content. (a) without HA, (b) 5% and (c) 10%.

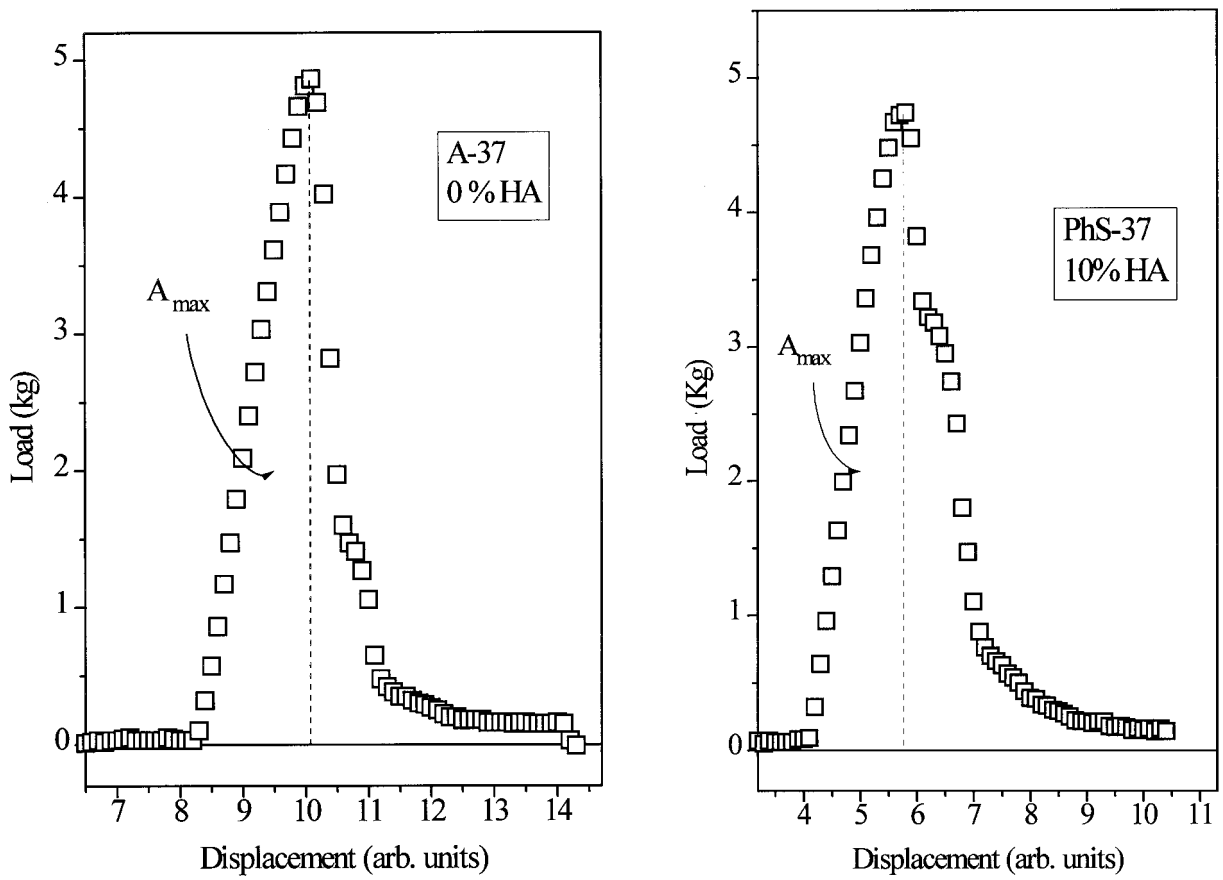

Figure 10 Load–displacement record. (a) A-37 specimen without HA, (b) 10% PhS-37 specimen and (c) 10% HA A-120 specimen.

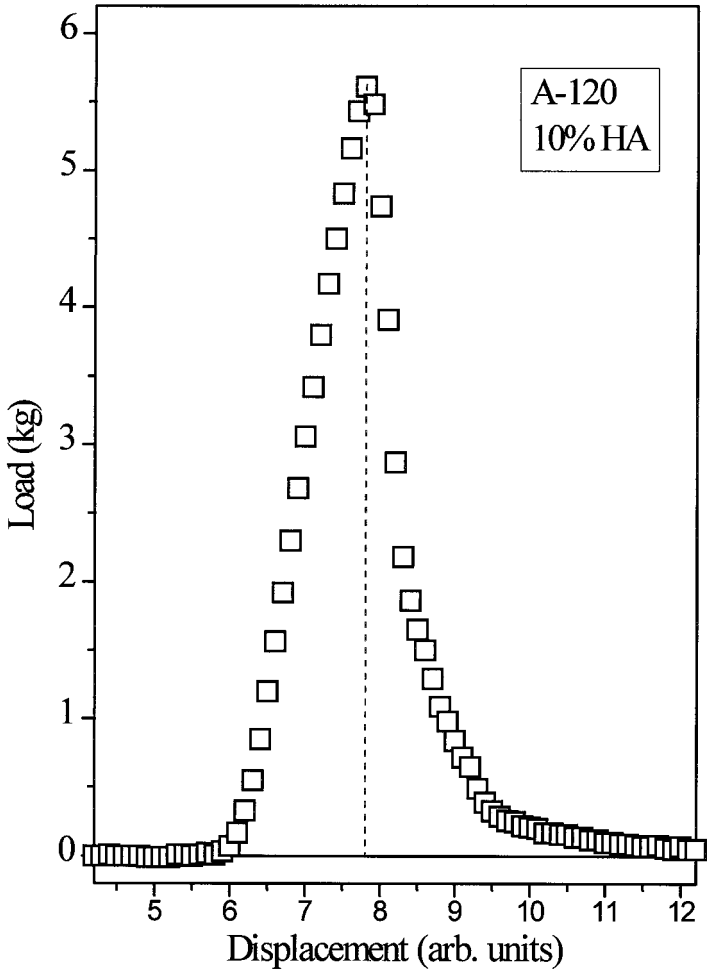

Figure 10 (Continued)

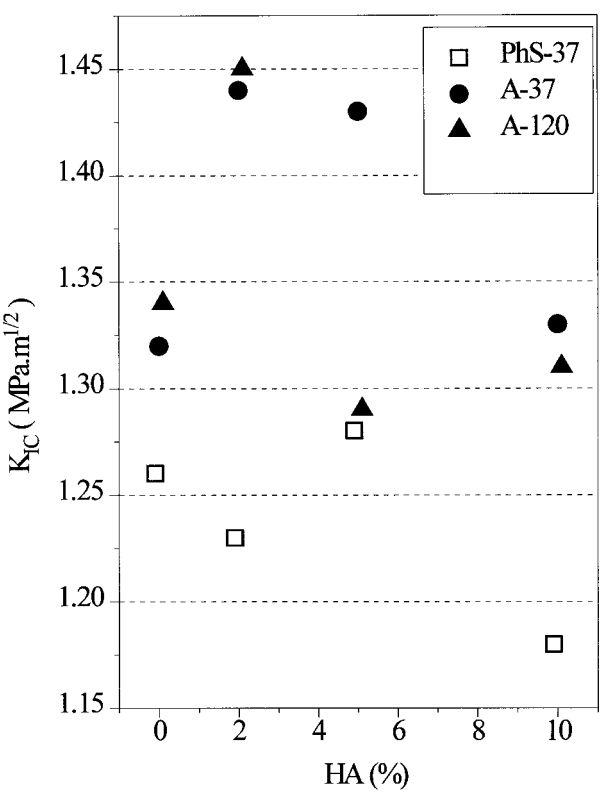

Figure 11 Stress intensity factor against HA content.

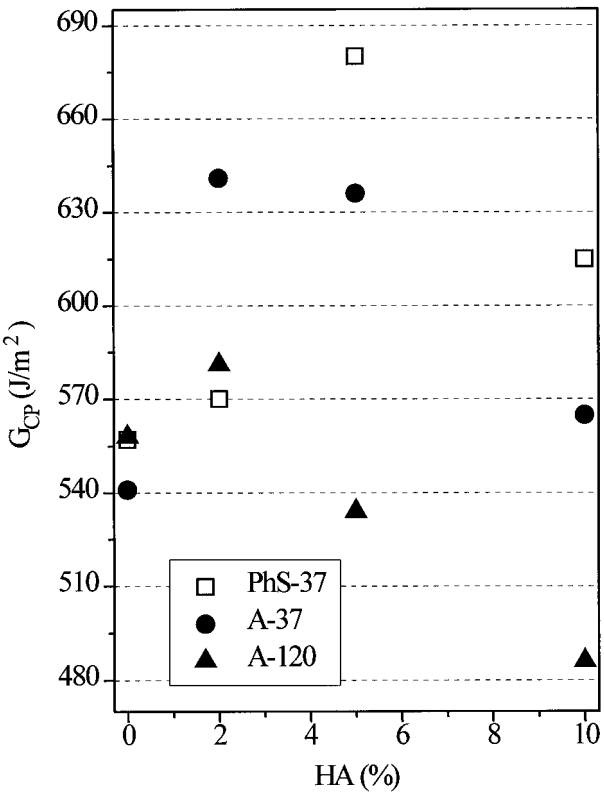

Figure 12 Propagation surface fracture energy against HA content.

TABLE IV Stress intensity factor K_{IC} (MPa m$^{1/2}$) and propagation value of strain energy release rate (J m^{-2}) of stored samples

HA	A-37		A-120		PhS-37	
(%)	K_{IC}	G_{CP}	K_{IC}	G_{CP}	K_{IC}	G_{CP}
0	1.32 ± 0.050	541 ± 33	1.34 ± 0.070	558 ± 19	1.26 ± 0.070	557 ± 43
2	1.44 ± 0.090	641 ± 70	1.45 ± 0.080	581 ± 54	1.23 ± 0.050	570 ± 44
5	1.43 ± 0.002	636 ± 63	1.29 ± 0.050	534 ± 35	1.28 ± 0.060	680 ± 33
10	1.33 ± 0.060	565 ± 59	1.31 ± 0.080	586 ± 74	1.18 ± 0.060	615 ± 44

propagation values of the fracture surfaces energies were found.

Fig. 12 and Table IV shows the tendency found for G_{CP} values. In all three programs there is a significant maximum in G_{CP}. The highest G_{CP}. were displayed by PhS-37 while the lowest porpagation fracture resistance were displayed by A-120 samples which agree with their lower content of plasticizer (water and residual monomer), which seems to induce more stable propagation.

4. Conclusions

Overall mechanical properties of composites based on acrylic cements and HA were not substantially affected by the addition of HA.

It was demonstrated that storage conditions and sample dimensions can affect the mechanical properties.

HA acted as a rigid filler slightly enhancing fracture resistance, flexural modulus and yield strain, up to a certain content. Beyond the latter limit, properties start to decrease since the addition of HA also affected the cement porosity.

Absorbed water acted as plasticizer leading to a decrease in mechanical properties.

The divergences in K_{IC} trends observed in literature may also be the result of the existence of an unstable propagation crack regime (crack arrests after the first fast growing), not reflected in the fracture initiation values, K_{IC}, which appears incomplete in describing the whole fracture behavior. G_{CP} approach resulted more accurate to represent the actual material behavior.

A modest, but statistically significantly, improvement in fracture resistance, i.e. K_{IC} and G_{CP}, was seen by reinforcing the cement with 2–5% of HA.

The highest propagation strain energies were exhibited by materials aged in PhS (except with 2% of HA) since the presence of water in the samples seems to induce a high degree of fracture stability.

Acknowledgment

The authors thank Subiton Laboratories for supplying the acrylic bone cements.

References

1. F. A. WEBER and J. CHARNLEY, *J. Bone Joint Surg.* **57 B** (1975) 297.
2. L. D. TIMMIE TOPOLESKI, P. DUCHEYNE and J. M. CUCKLER, *J. Biomed. Mater. Res.* **29** (1995) 299.
3. D. N. HILD and P. SCHWARTZ, *J. Mater. Sci.: Mater. Med.* **4** (1993) 481.
4. C. M. RIMNAC, T. M. WRIGHT and D. L. MCGILL, *J. Bone Joint Surg.* **68-A** (1986) 281.
5. C. T. WANG and R. M. PILLIAR, *J. Mater. Sci.* **24** (1989) 3725.
6. A. CASTALDINI, A. CAVALLINI and D. CAVALCOLI, in ''Biomaterials and clinical applications,'' edited by A. Piezoferrato, P. G. Marchetti, A. Ravaglioli and A. J. C. Lee, (Amsterdam, 1987).
7. M. JARCHO, C. BOLEN, M. THOMAS, J. BOBICK, J. KAY and R. DOREMUS, *J. Mater. Sci.* **11** (1976) 2027.
8. M. JARCHO, J. KAY, K. GUMAER, R. DOREMUS and H. DOBRECH, *J. Bioengng* **1** (1977) 79.
9. P. W. BEAUMONT and R. J. YOUNG, *J. Biomed. Mater. Res.* **9** (1975) 423.
10. B. PASCUAL, M. GURRUCHAGA, I. GOÑI, M. P. GINEBRA, F. J. GIL, J. A. PLANELL, B. LEVENFELD, B. VASQUEZ and J. SAN ROMAN, *J. Mat. Sci.: Mater. Med.* **6** (1995) 793.
11. G. LEWIS, *Biomaterials* **13** (1992) 225.
12. J. A. JOHNSON and D. W. JONES, *J. Mater. Sci.* **29** (1994) 870.
13. J. SHEN, C. C. CHEN and J. A. SAVER, *Polymer* **26** (1985) 511.
14. J. L. HAILEY, I. G. TURNER, A. W. MILES and G. PRICE, *J. Mater. Sci.: Mater. Med.* **5** (1994) 617.
15. P. MONTEMARTINI, C. VALLO and T. CUADRADO, in Actas del Simposio Arg. de Polímeros, (Huerta Grande, Cordoba, Argentina, Universidad Nacional del Litoral, 1995), p. 279.
16. A. FANOVICH and J. M. PORTO LOPEZ, *Anales Asociación Química Argentina* **83** (1995) 343.
17. P. MONTEMARTINI, A. FANOVICH, C. VALLO, J. M. PORTOLOPEZ and T. CUADRADO, J. Biomed. Mater. Res. Appl. Biomater. (in press).
18. J. WILLIAMS and M. J. CAWOOD, *Polymer Testing* **9** (1990) 15.
19. M. J. ADAMS, D. WILLIAMS and J. G. WILLIAMS, *J. Mater. Sci.* **24** (1989) 1772.
20. C. I. VALLO, T. R. CUADRADO and P. M. FRONTINI, *Polym. Int.* **43** (1997) 260.

Received 22 April 1997
and accepted 19 August 1998